11th INTERNATIONAL SYMPOSIUM ON COMPRESSOR & TURBINE FLOW SYSTEMS THEORY & APPLICATION AREAS SYMKOM 2014 IMP^2, Lodz, 20 - 23 October, 2014

EU-Norsewind – Delivering offshore wind speed data for renewable energy

Matthew T Stickland [1*], Andrew Oldroyd [2], Charlotte Bay Hasager [3], Thomas Scanlon [1]

[*] matt.stickland@strath.ac.uk

[1] *Department of Mechanical and Aerospace Engineering, University of Strathclyde, Glasgow, UK E-Emails; matt.stickland@strath.ac.uk, tom.scanlon@strath.ac.uk*

[2] *Oldbaum Services, Stirling FK9 4NF, UK Email; andy@oldbaumservices.co.uk*

[3] *DTU Wind Energy, Technical University of Denmark, Frederiksborgvej 399, 4000 Roskilde, Denmark Email; cbha@dtu.dk*

Abstract:

Offshore wind is the key area of expansion for most EU states in order to meet renewable energy obligations. However, a lack of good quality offshore wind resource data is inhibiting growth in this area. To address this issue the NORSEWInD project was established in 2008 to develop the methodology for creating a wind atlas from remote sensing satellite data which is available in the public domain. This paper gives an overview of the methodology developed and includes the so-called "NORSEWInD standard" for comparing LIDAR and mast wind data, the technique for estimating the flow distortion measured around offshore platforms by LiDARs using wind tunnel and CFD data and observations of the vertical wind profile shear exponent at the hub height of off shore wind turbines.

Keywords:

LIDAR; offshore winds; remote sensing; wind energy; wind resources

Introduction

Wind Resource data is a key component for all wind energy projects. As the deadline for the EU's promised 20% reduction in carbon emissions by 2020 fast approaches, there is need for accurate information on ocean winds for offshore wind farms and turbine clusters in the Northern European Seas. In large offshore wind farm projects the economic risk is considerably reduced when accurate wind data are available at hub height for a minimum of one year. For a decrease in uncertainty on the predicted mean wind speed at hub height of 0.1 m/s there is an estimated saving worth around £10 million per year for 25 years for a large offshore wind farm project according to industry experts [1]. Wind data are usually acquired by mounting cup and vane anemometers on a mast at hub height at the proposed wind farm location. On shore this is feasible but offshore the costs involved in erecting a mast to 100m above mean sea level (AMSL) are prohibitive. The cost of installing and operating tall meteorological masts has increased in recent years and currently has a price tag of around £10 million for a two-year measurement campaign, thus alternatives using remote sensing are desirable [reference]. The purpose of this article is to present the lessons learned during the five year EU FP7 funded project NORSEWinD which developed the techniques necessary for wind resource assessment offshore using both LiDAR (Light Detecting And Ranging) and satellite based remote sensing techniques.

The benefit of choosing LiDAR remote sensing technology was the ability to measure wind data at higher levels than possible with a meteorological mast and at the same time to ensure high accuracy in wind speed measurements at relatively low cost. The need for improved knowledge on winds at higher levels is twofold: Firstly modern wind turbines, especially those deployed offshore, are increasing in dimension and the flow across their large rotors is not well-explained by hub height winds alone [1]. Secondly the marine atmospheric boundary layer and its temporal behavior at higher levels is poorly known. Thirdly there is a need for improved parameterizations of the marine vertical wind profiles in order to improve modeling of offshore winds for wind energy resource assessment [2] and to experimentally evaluate atmospheric wind resource models using predictions against measured offshore winds [3].

Wind LiDAR remote sensing technology has had a very rapid growth and it has become widely used within the wind energy community in recent years. The early experiments at DTU Wind Energy (formerly Risø) with a focused continuous wave (cw) Doppler wind LiDAR took place onshore over flat terrain at Høvsøre near the tall meteorological mast in 2003 [4]. This was followed by an experimental deployment offshore on the Fino-1 platform in 2005 [5], the Nysted 1 offshore wind farm transformer platform in 2006 [6] and the Horns Rev 1 offshore wind farm transformer platform in 2007 [2]. At all three offshore sites meteorological masts were located nearby and the concurrent meteorological observations were used for comparisons to the LiDAR observations. The data analysis from these early offshore experiments gave promising results. This fact stimulated the idea for using an array of wind profiling LiDARs in the Northern European Seas where the majority of European offshore wind farms have been either developed or are in the planning stage but where the knowledge of the wind resources is limited.

In the EU FP7 Northern Sea Wind Index Database (NORSEWiND) investigation from 2008 to 2012 [7] nine LiDARs were deployed on offshore platforms in the North Sea and one LiDAR was deployed near the coast of the Norwegian island of Utsira. The research objectives of the NORSEWiND project included systematic analysis of the marine wind shear observed from the LiDARs [8] and investigation of the flow distortion around the offshore platforms [9]. It was important to investigate the platforms' influence on the free stream wind speed profiles at hub height to see if the LiDAR data was affected by flow distortion. Other results from the project included a wind atlas based on numerical modeling and satellite data [3,10–15]. The wind atlas is publicly available from the project web-site [7].

The purpose of this article is to present the lessons learnt on the LiDAR measurement technique, deployment strategies and pre- and post- deployment validation including the definition of data quality acceptance levels: the so-called "NORSEWiND standard". Also the requirements for installation setup, the data availability, system consistency and multi-year performance are described. The work demonstrates the data management strategy for reliable application of LiDAR data. The measurement of flow distortion by the platforms using sub-scale models in a wind tunnel and computational fluid dynamics is described with the aim to clarify the level of flow distortion influence on the LiDAR wind profile observations at hub height. A total of 77,491 hours, equivalent to 107 operational months, of wind profile data from 10 LiDARs over the period July 2009 to April 2012 were recorded. The data are stored as 10-min average values in a MySQL database [7].

Wind Resource Assessment

From observation it is common knowledge that wind comes from all directions and is never steady. Bearing in mind the variability in direction and strength of the wind how is it possible to predict how much a wind turbine might produce in one year? As discussed by Wager [1] assessment of the actual wind resource at a planned wind turbine farm site is essential to ensure that the proposal is economically viable. There are many books which discuss the method by which wind resource is assessed but, for completeness of this paper, the process will be discussed briefly.

To estimate the wind resource the wind speed and direction should be measured at the wind farm location for at least a year with 10 year statistics to help assure viability. Typically the measured wind speed is time averaged over ten minutes and the ten minute averages binned over discrete speed ranges to create a plot of probability density function against wind speed, figure 1. Once this distribution has been created a Weibull distribution, equation 1, is fitted through the data.

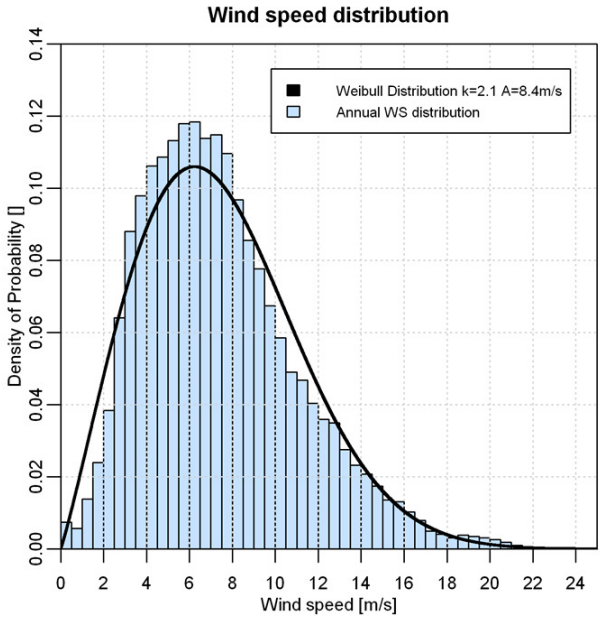

Figure 1. Typical wind speed distribution with Weibull distribution fitted to the data.

$$p(U) = \left(\frac{k}{A}\right)\left(\frac{U}{A}\right)^{k-1} exp\left[-\left(\frac{U}{A}\right)^{k}\right] \quad (1)$$

Where k is a shape factor and A is a scale factor. From the Weibull distribution it is possible to calculate the mean wind speed, equation 2 and 3, the standard deviation, equation 4, and the turbulence intensity, equation 5.

$$\overline{U} = A\Gamma\left(1 + \frac{1}{k}\right) \quad (2)$$

$$\Gamma(x) = \int_0^\infty e^{-t}t^{x-1}dt \quad (3)$$

$$\sigma_u{}^2 = \overline{U}^2\left[\frac{\Gamma\left(1+{}^2/_k\right)}{\Gamma^2\left(1+{}^1/_k\right)} - 1\right] \quad (4)$$

$$TI = \frac{\sigma_u}{\overline{U}} \quad (5)$$

Given the planned wind turbine's power performance curve, $P_w(U)$, figure 2, and the Weibull distribution of the wind resource, p(U), it is possible to calculate the annual power production, equation 6, and the capacity factor, equation 7, where P_R is the rated power of the turbine.

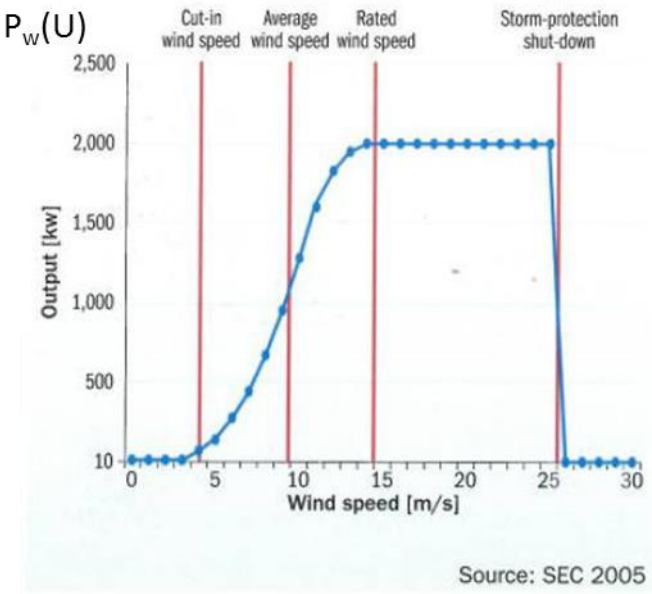

Figure 2. Typical wind turbine power performance curve

$$\bar{P}_w = \int_0^{\infty} P_w\,(U) p(U) dU \tag{6}$$

$$CF = \frac{\overline{P_w}}{P_R} \tag{7}$$

The NORSEWInD Study Area

Nine LiDARs were deployed on offshore platforms. One lidar was deployed on the coast of the island of Utsira. Figure 1 illustrates the locations.

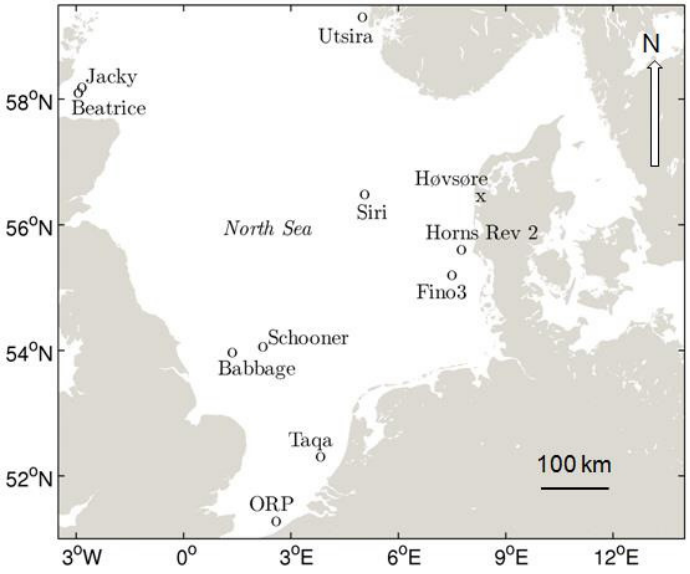

Figure 3. Map of lidar positions and the Høvsøre test site [7].

The LiDARs were operated on the platforms over the period from July 2009 to April 2012. Only during a short period in the summer of 2011 did all LiDARs but one operate simultaneously. An overview of the periods of operation is given in Figure 2. The reasons for the different start times and durations of observations were due to practical issues and logistics.

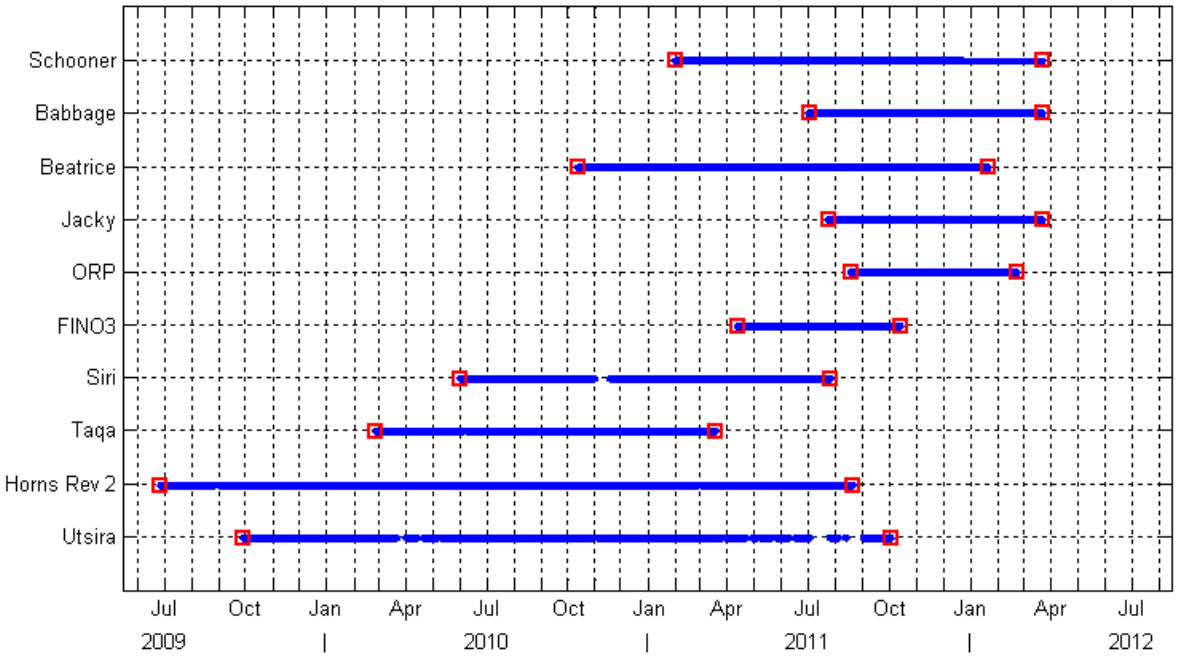

Figure 4. Overview of observation period from the LiDARs.

Deployment Strategies at Offshore Platforms

All LiDARs in the NORSEWiND project were planned to provide stand-alone wind profile observations offshore over many months of operation with no nearby meteorological masts for comparison during the offshore deployment. This prompted a need for careful pre- and also post-deployment validation. Prior to the pre-deployment validation a standard for the data quality acceptance levels for the NORSEWInD LiDAR systems was defined. This is the so-called "NORSEWInD standard" and the details are given in Table 1 [reference].

Table 1. Data quality acceptance levels for NORSEWInD lidar systems. u stands for wind speed.

Parameter	Criteria	Ranges (Height and Speed)
Absolute error	<0.5 ms^{-1} for 2 < u < 16 ms^{-1} Within 5% above 16 ms^{-1} Not more than 10% of data to exceed those values	All valid data
Data availability	Assessed case by case Environmental conditions dependency	All valid data
Linear regression Slope	Slope between 0.98 and 1.01 <0.015 variation in slope between u-ranges (b) and (c)	Heights from 60 to 116 m u-ranges: (a) 4–16 ms^{-1}, (b) 4–8 ms^{-1}, (c) 8–12 ms^{-1}
Linear regression Correlation coefficent (R^2)	>0.98	Heights from 60 to 116m u-ranges: (a) 4–16 ms^{-1},

Access to the LiDARs at the offshore platforms was limited therefore it was necessary to carefully plan their deployment and operation. The LiDARs were selected by the industrial partners and encompassed focused cw Doppler wind LiDARs of the type ZephIR® [16,17] and pulsed wind LiDARs of the type WindCubeWLS7® [18,19]. Dependent upon the height of the platform at which each lidar was installed there were specific deployment plans for the two types of LiDARs. The key aim was to observe wind profiles without significant flow distortion from the platform and to observe wind speed and direction at several heights in free stream conditions. It was decided as most important to observe wind speed at 100 m above mean sea level (AMSL) as it was expected to be close to the hub heights of future offshore wind turbines. A wind turbine with a rotor diameter of 120 m will sweep from 40 to 160 m AMSL. The wind profiles were planned to be observed within this height range in steps of 20 m, typically at 5 or 6 heights for the ZephIRs and at 10 heights for the WindCubes.

The deployment requirements for each platform or rig included technical and legal considerations. It was essential to ensure the installation would be at a suitable location with a level and vibration-free position and the mounting would be with free field of view for all laser beam directions as measurement beams could potentially have been disturbed by the rig, cranes, derricks, building, etc. Figure 5 shows some LiDARs in situ to demonstrate the selected installation spots on oil and gas rigs.

Figure 5. Photograph of selected LiDARs on installation platforms.

For more information about the difficulty of installing and operating the LiDARs on the offshore platfroms refer to Hassegar et al [39]

Flow Distortion due to Offshore Platform and Terrain

Nine of the lidars were deployed on offshore platforms. These platforms included large gas and oil drilling rigs with tall derrick structures (Beatrice, Siri, Taqa, ORP), smaller unmanned production platforms (Jacky, Schooner, Babbage), wind farm transformer stations (Horns Rev 2 in the North Sea, Denmark) and a platform mounted meteorological mast (Fino3 in the North Sea, Germany). One lidar was deployed on the coast of the island of Utsira, see [8] for details. Common to all installations was the risk of flow distortion around the structures or influence from the surrounding landscape on the observed wind profile. The aim of the NORSEWInD project was to accurately observe free stream winds at hub height; thus it was desirable to minimize the flow distortion on the lidar wind profile observations by selecting the observational heights with care. In certain cases it could, however, become necessary to correct the wind profile observations.

To investigate the flow distortion around the platforms and to validate the Computational Fluid Dynamic (CFD) simulations, measurements in a low speed wind tunnel were made with a calibrated DANTEC Streamline constant temperature (CTA), triple wire anemometer mounted on a three dimensional traversing rig as shown in the diagram of Figure 6.

By traversing the hot wire probe vertically above the location of the simulated lidar the velocity profile in a vertical line above the rig could be determined. This velocity profile was then compared with the results of the CFD simulation of the rig. Initially, to create a base line against which the effect of the rig on the flow field could be assessed, the flow in the wind tunnel was traversed without the rig model present in the tunnel. The measured vectors were then non-dimensionalised by a reference wind speed measured by a single hot wire probe upstream and to the right of the proposed model location, with due care taken to ensure the reference speed was outside any likely flow disturbance that might be caused by the presence of the rig model. This provided the non-dimensional, undisturbed, free stream velocity at the measurement locations above the rig for neutral conditions.

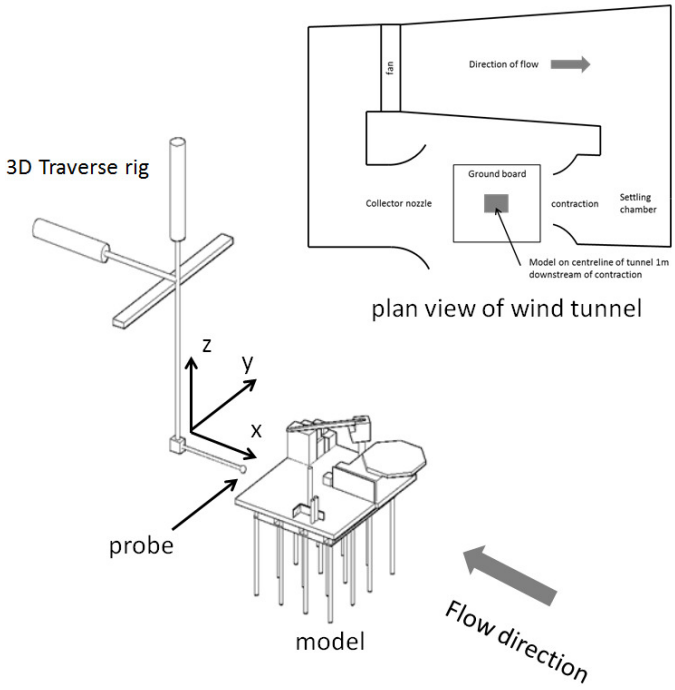

Figure 6. Diagram of constant temperature (CTA) probe traverse system showing the wind tunnel coordinate system and a plan view of wind tunnel layout.

Simulations were undertaken at model scale and full scale to identify any issues regarding Reynolds number effects in the subscale wind tunnel tests and none were found. Length scale for oil production platforms was typically between 0.5 m and 1m and 1.5 m for models of the island. Tunnel free stream

speed was 15 ms^{-1} in all cases. Platform models were typically 100th scale and 1,250th scale of the platforms and island, respectively. The CFD simulations were carried out for turbulent flow and the turbulence intensity in the 1.5 m low speed wind tunnel is approximately 1%. The k-omega turbulence model was selected because the model is a mature and established algorithm intended for general use with external flows [21]. To confirm the validity of the CFD simulation and to evaluate the most appropriate turbulence model the data collected by the hot wire traverses above the rig were compared to the CFD data at the same locations using a range of turbulence models including the k-ω and the standard k-ε model.

The rig was then placed in the tunnel and the velocity profiles above the rig measured. Comparing this data with the data acquired in the empty tunnel the effect of the presence of the rig on the undisturbed flow field was determined. Figure 7 shows the results of four traverses above a rig with the flow approaching the rig from different azimuthal angles. The X on the plan form view of the rig shows the location above which the probe was traversed in the positive Z direction. Probe heights were normalised by the height of the rig deck and the speed was normalised by the free stream velocity of the wind tunnel [22].

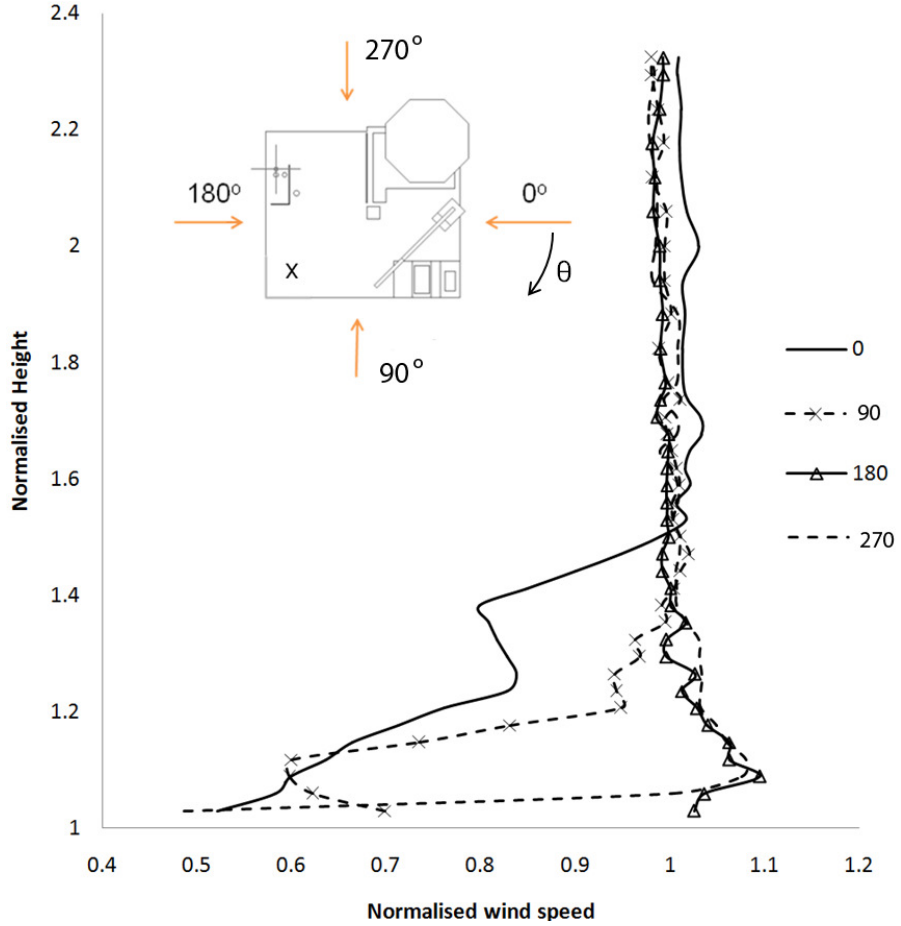

Figure 7. Non-dimensional velocity magnitude profiles measured above the platform with the flow approaching from four different azimuth angles.

The data from the wind tunnel tests served two purposes: to assess the height above the platform that a point measurement device, such as a cup and vane anemometer, might be affected by flow distortion, and to verify CFD simulations which were required to assess the effect of flow distortion on the measurements made by lidars. By rotating the platform 360° in the wind tunnel and measuring the velocity profiles, the boundary where the flow velocity magnitude was within a certain percentage of the free stream velocity could be determined, see Figure 9. The result of this analysis for a number of platforms is shown in Table 6. The CFD model results compared well with the wind tunnel experiment [9,23] and were used to determine the effect of flow distortion on the measurements made by the lidars

both onshore and offshore. The effect of flow distortion on the cup and vane type anemometer, being essentially a point measurement, is easily understood and measured. However, remote sensing devices, such as lidars and sodars, determine the wind vector from a spatially averaged set of measurements.

Some attempts have been made to measure the effect of flow distortion on lidars in complex terrain as might be found when measuring in hilly or mountainous terrain [2,5,19,24–27]. In the WAsP Engineering software [28], a program for wind site assessment, a script is available that accounts for the error due to the flow distortion created by orography when scanning conically with two types of lidars [25]. The authors of [8] investigated the influence of the landscape to the wind profile observed by the lidar on the island of Utsira and found significant influence to the wind profile at all levels and with clear azimuthal dependence. However, the effect of the flow distortion on lidars in close proximity to large structures, such as buildings and oil rigs, had not been investigated to date. To understand the difficulty of estimating the effect of flow distortion on the measurements made by a lidar it is necessary to understand the fundamental difference between the point measurement of a cup anemometer and the spatially averaged velocity measurement of a lidar.

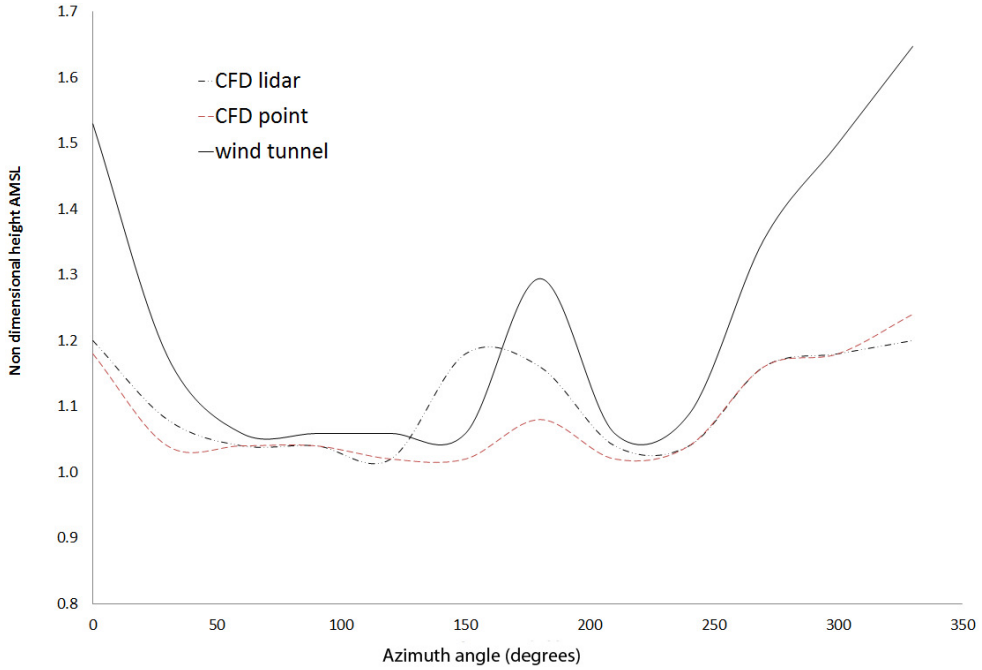

Figure 8. Height above rig required for 99% free stream velocity magnitude as a function of the azimuth angle from wind tunnel and Computational Fluid Dynamic model results.

The measurement technique employed by lidar systems relies on spatially averaged line of sight velocity measurements of the flow field. To measure a 3D velocity vector three or more line of sight velocity vectors are required. Depending on the instrument and the technique employed the number of line of sight vectors can be as low as 4 (WindCube) or as high as 150 (ZephIR). In order to assess the likely impact of an inhomogeneous flow field on such measurement techniques it was necessary to simulate more than a single point in the flow and assess any interference that might exist at each measurement point. Only when this interference at every measurement location had been found the effect on the final velocity vector could be determined.
To assess the effect of a platform's flow distortion on the lidars, the flow field over each platform was simulated using CFD and so the measurements performed by a scanning lidar. In this way the extent to which the platform affected the measurements made by a lidar mounted on that platform could be determined. The CFD data also provided information on the distortion observed by a point measurement device such as a cup anemometer.

Table 6 gives he height above lidar installation level and AMSL for undisturbed flow measurement from wind tunnel and CFD point measurement and by lidar based simulation from CFD where u is the

magnitude of the wind velocity and θ is flow angle in the horizontal plane. The values in the columns are height in meters AMSL at which this measurement is unaffected (±2.5% free-stream) by distortion. Numbers in brackets are the height at which distortion is negligible non-dimensionalised by the platform height. Horns Rev 2, a transformer platform, caused distortion in the magnitude of the velocity vector in the horizontal plane, U_{mag}, up to a height equivalent to that of the rig whereas Schooner created distortion up to 0.2 times the rig height only. The extent to which distortion was created appeared to be a function of the solidity of the rig. The open lattice type structures created significantly less distortion than the more solid structures such as Horns Rev 2. It should be noted that the CFD simulations indicated that the lidar measurements were less susceptible to flow distortion than a point measurement at the same height. Also of note was the height to which the island of Utsira created distortion.

Table 2. Height above lidar installation level and AMSL for undisturbed flow measurement from wind tunnel and CFD point measurement.

			Height above Lidar in m (Height Normalized by Rig Height)					Height AMSL for 2.5% Free-Stream	
Platform	Rig Height (m)	Lidar Height (m)	Wind Tunnel	CFD Results				CFD Results	
			Point	Point		Lidar		Lidar	
			u	u	ϑ	u	ϑ	u	ϑ
Babbage	42	42	33 (0.8)					75	
Beatrice	62	42.5	64 (1.0)	30 (0.5)	>64 (1.0)	34 (0.5)	59.5(1.0)	76.5	102
HornRev 2	26	26	30 (1.2)	44 (1.7)	57 (2.2)	25 (1.0)	55 (2.1)	50	80
Jacky	28	28		20 (0.7)	19 (0.7)	10 (0.4)	18 (0.6)	38	46
Schooner	38	36.25	24 (0.6)	24 (0.6)	35 (0.9)	9 (0.2)	24 (0.6)	39	54
Taqa	31.4	30	37 (1.2)	30 (1.0)	36 (1.1)	33 (1.1)	27 (0.9)	63	57
Utsira	26	26		108 (4.2)	192 (7.4)	150 (5.8)	300 (11.5)	176	326

From the simulation of the lidar measurements in the distorted flow field it was possible to calculate correction factors and addends that could be applied to the data measured by the lidars situated on the offshore platforms. To correct the magnitude and direction of the free stream velocity vector in the horizontal plane, u and θ respectively, to the undisturbed free stream values Equations (1) and (2) were derived. In the simulation the values of u-free stream and θ-free stream in the undisturbed flow were known and the measurements made by a lidar, u-lidar and θ-lidar in the distorted flow field could be determined from the lidar simulation. Substituting these values into Equations (1) and (2) allowed the corrections, cff_u and cff_θ, to be determined.

$$u_{\text{free stream}} = cff_u \times u_{\text{lidar}} \tag{8}$$

$$\theta_{\text{free stream}} = \theta_{\text{lidar}} + cff_\theta \tag{9}$$

Correction factors were a function of height and free stream flow angle as shown in Figure 10. Flow corrections were only applied to data where the correction required was greater than 2.5%, for the flow magnitude and 0.5° for the flow direction as this was considered to be the limits of the accuracy of the

CFD simulation data. Corrected and uncorrected data were stored separately in the database so that either version of the data could be analysed as required.

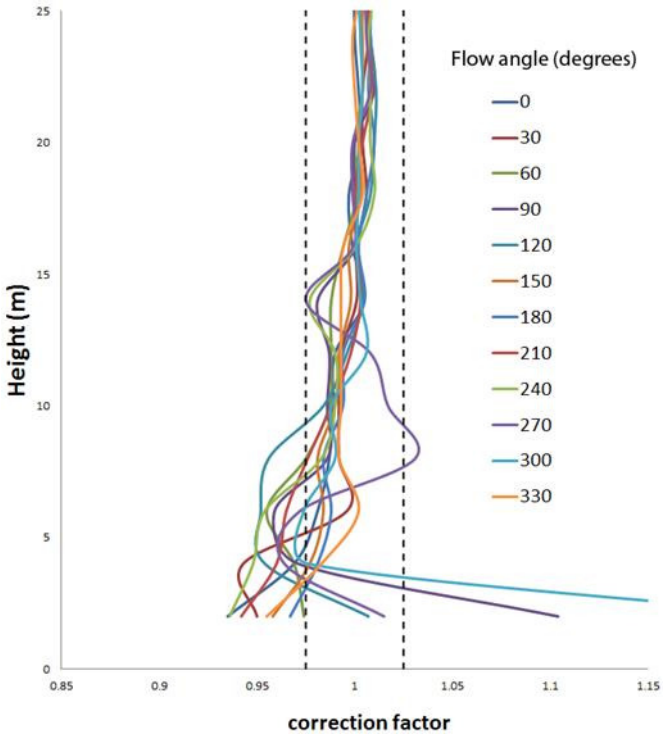

Figure 10. Correction added to the azimuth angle in the horizontal plane up to 50 m above rig height over 360° free stream azimuth flow angle in 30° steps.

Determination of wind shear profile

One of the most significant obstacles in the use of remote sensing satellite data to determine wind resource offshore is the method by which the satellites determine the wind speed [references]. Both synthetic aperture radar and scatterometer satellites determine the wind speed at sea level and require some form of algorithm to correct this wind speed to heights AMSL. The determination of the shear layer profile is usually established by computational modelling which is unsatisfactory. However the LiDAR measurements made during the NORSEWInD campaign allowed the determination of the offshore shear profile as discussed in the following section.

All NORSEWInD wind lidars were able to observe winds at 100 m and higher. Most of them were WindCube systems (Table 4), i.e., pulsed lidars; thus the availability of data decreases with height (Figure 5). In order to maximize the amount of data we decided to estimate the wind shear from the two closest wind speed observations to the 100 m height. The wind shear is estimated as the value of the shear exponent α of the power law:

$$\frac{u_1}{u_2} = \left(\frac{z_1}{z_2}\right)^{\alpha} \tag{10}$$

where u is the magnitude of the wind speed, z the height, and 1 and 2 referred to two levels. α can then be estimated as:

$$\alpha = \frac{z}{u}\left(\frac{du}{dz}\right) \approx \frac{z}{u}\left(\frac{\Delta u}{\Delta z}\right) \tag{11}$$

Equation (10) is important because one can relate α to Monin-Obukhov similarity theory and will find that (see [8,32]):

$$\alpha = \frac{\Phi_m}{\ln\left(\frac{z}{z_0}\right) - \psi_m} \tag{12}$$

where z_0 is the surface roughness length and Φ_m is the dimensionless wind shear, which is a function of the dimensionless stability parameter z/L and also some sort of the derivative with respect to height of ψ_m and L is the Monin-Obukov length. Based on Equation (5), we therefore expect that within the surface layer α is a function of height and will vary as z_0 increases with wind speed (among others) over the sea and ψ_m depends on the atmospheric condition. The relationship of α and stability was investigated from offshore mast data Fino-1 at heights below 80 m and compared to Large Eddy Simulation results [33] and the dependence of the power-law exponent on surface roughness and stability in a neutrally and stably stratified surface boundary layer was described by [34]. Recently [35] compared one year of LiDAR data to Fino-1 meteorological data, and [36] studied wind shear from the wind LiDAR observations at Fino-1 as a function of stability, and [37] compared data to meteorological data in upland terrain.

Figure 11. Distribution of α at a height close to 100 m, estimated using Equation (10)

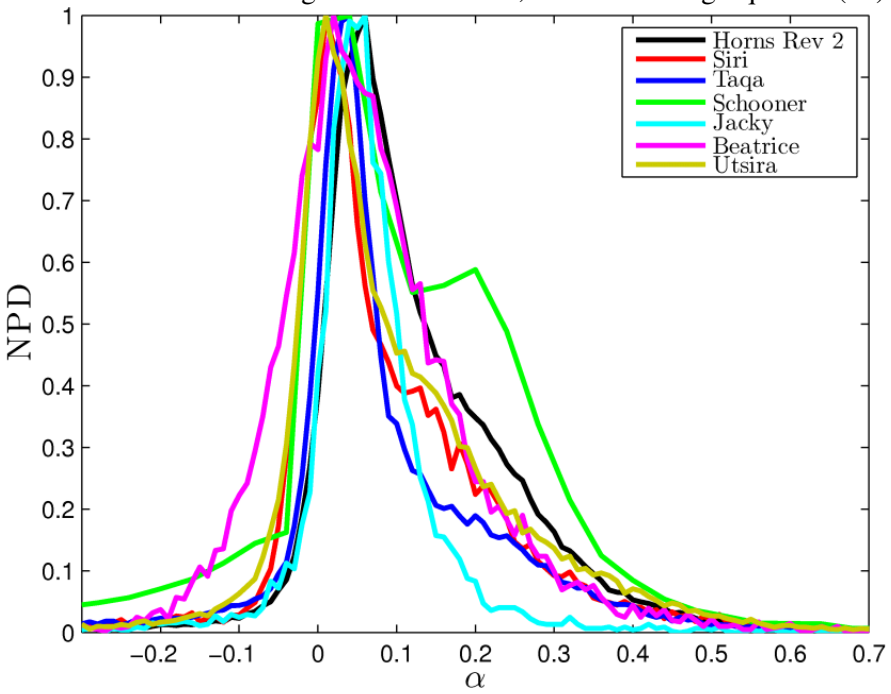

It was noted that:

- For all the nodes, there is a broad range of α-values, mostly in the positive side of the distribution, which contrasts with the common value of 0.2 used for load calculations offshore. See [32] for further discussion of the α-value.

- A higher amount of positive α-values was found since wind speeds are generally higher above than below 100 m, as expected, but at all nodes it is also observed a significant amount of negative α-values. The latter are normally found either under conditions where the atmosphere is very unstable and the wind speed does not change much with height (due to the nature of the atmosphere dynamics higher wind speeds are observed below 100 m) or conditions where the atmosphere is very stable and so low-level jets or shallow boundary layers influence the wind profile so that it bends backwards. It can be seen that predictions of the distribution of α using Equation (3) might only fit a range of positive values (no negative values can be estimated from it, although the conditions are very unstable and the sea roughness is high).
- Most distributions peak on a positive value between 0 and 0.05. The clearest exception is Horns Rev 2, which was in the wake of the wind farm most of the time which increased the wind shear at this particular height [8].
- Most distributions lie on each other; the greater exceptions are those at Jacky and Beatrice (the two with the fewest high-quality data for the analysis by far), and Schooner that shows a bump at about α = 0.2 which might not be real since a systematic problem with data was found, although the data shown should be "correct" according to the NORSEWInD standards (see Table 1).

Wind Atlas creation

Hasager et al [40] used the NORSEWInD procedure to create a wind resource map in a case study of the Baltic Sea east of Denmark, figure 12. To create the wind atlas multiple wind speed maps from at sea level EnviSat were taken over the focus zone, figure 12.

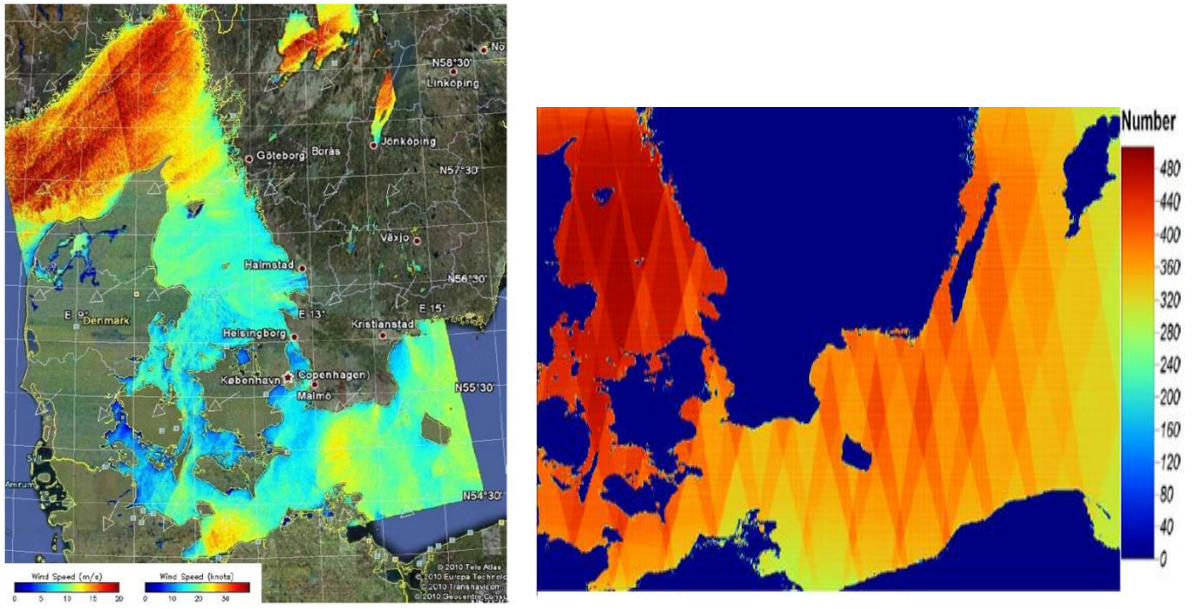

Figure 12. Sea level wind speed map Jan 1 2010 20:48 UTC (left) and number of scenes (right) [40]

The sea level wind speed data was extrapolated from sea level to hub height using the shear profiles developed above and a Weibull distribution fitted to the data to produce contour plots of Weibull A and Weibull k, figure 13.

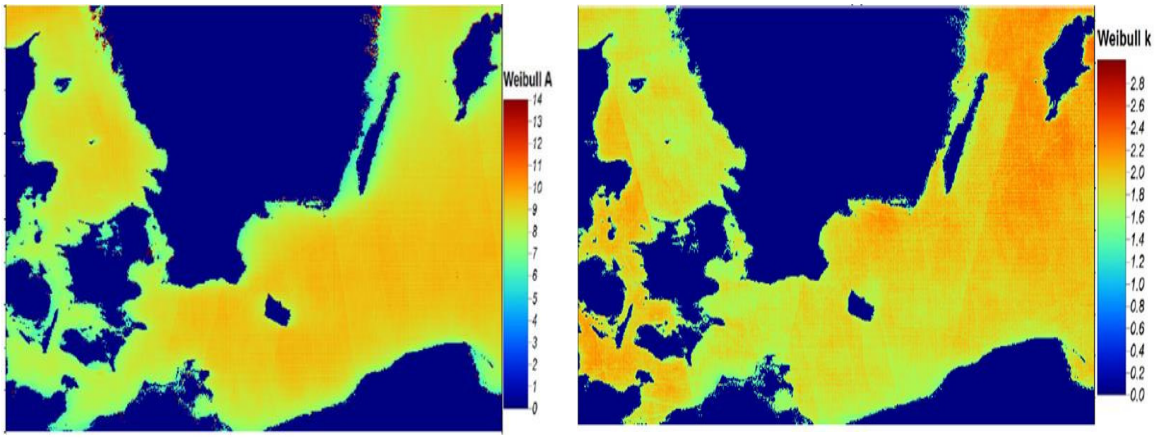

Figure 13. Contour plots of Weibull A (left) and Weibull k (right) [40]

From the Weibull data contour plots of power density over the focus zone were determined, figure 14, and the results compared with similar data calculated from meteorological masts in the focus zone, table 2.

Table 2. Comparison of Wiebull A, K and power density from satellite and met mast data [40].

FINO-2	Mast (WAsP)	SAR (WAsP)	SAR (M.L.)	Difference (%) (WAsP-WAsP)	Difference (%) (WAsP-M.L.)
Mean wind speed (m s^{-1})	8.12	8.17	8.16	0.5	0.6
Weibull A (m s^{-1})	9.00	8.72	9.21	2.3	3.1
Weibull k (−)	2.31	1.94	1.93	−16.9	−16.0
Power density (W m^{-2})	521	559	670	7.3	28.6
N (-)	146,910	409	409	-	-

Discussion

The joint effort of the NORSEWInD team has resulted in new knowledge and lessons learnt with regard to observation of hub height wind measurements for wind energy using wind profiling LiDARs on offshore platforms and at the coast. The new knowledge includes three major issues on the device performance:

- The long term performance consistency for the wind profiling LiDARs employed is good. The so-called “NORSEWInD standard” pre-deployment validation showed excellent results for most of the LiDARs. Eight LiDARs were tested. The post-deployment validation tested four LiDARs and showed only minor deviations from the pre-deployment results. The results are

very encouraging. They indicate that the devices have a high absolute accuracy after 6 to 26 months of deployment in the harsh offshore environment. Considering that the need for new bankable wind data for offshore wind farm projects is high wind profiling LiDARs appear to be a suitable candidate for this task in the future.

- The system consistency of the two types of LiDARs used is encouraging. There are several differences in two types of LiDARs including the number of observational levels, the difference in volumes of air observed and the sensitivity to cloud and fog, see [8] for further details. Despite the differences both types of LiDARs passed the "NORSEWInD standard" and had similar post-deployment validation results. For winds at hub height both systems appear to perform well.
- The system availability for the devices when deployed offshore was lower than is typical on land. Onshore it ranged from 85% to 100% with an average of 95% but is typically higher at sites with a better power supply. The data availability offshore ranged from 73% to 97% with an average of 89%. Data availability is typically higher at sites with higher aerosol concentration. System availability may be improved by providing better training to the rig personnel in operating and maintaining the devices. However, on some platforms there were no personnel. Otherwise it is recommended to improve the system reliability by the manufacturers designing future devices which require reduced operational care. Without some type of improvement on the system and data availability there is risk of insufficient long term observations necessary for accurate wind resource assessment when based on unmanned platforms offshore.

The new knowledge gained on flow distortion around the offshore platforms using both sub-scale models in a wind tunnel and CFD modeling indicates that the practical use of even rather bulky offshore structures is acceptable for observing free stream winds with lidars at hub height and below. A rough guide is that the flow is not significantly distorted above 2.4 times the deck height. It is clear that neither the wind tunnel experiments, nor CFD modeling is a final proof. It is therefore important to recognize that a critical analysis of the specific wind profiles observed on the platforms should always be performed in order to further verify that the wind information is trustworthy [8].
Although the hub heights and rotor diameters are growing, the lower tip height is not changing. This is fixed by the consenting authority and is usually in the order of 30 m AMSL. At this height it is unlikely a pulsed system (unless inclined and hence well outside potential flow distortion effects) will be able to acquire a signal. A cw system would be able to acquire a signal, however, if a larger host platform is used, then the observation would most likely be higher than the lowest tip height. In short we would not expect to correct for lower tip height values even using flow correction factors for wind lidar observations.

The major lessons learnt from the offshore deployment are technical and legal issues. In a research and demonstration project such as NORSEWInD legal issues with the platform owners took a while in several cases. However, it is the technical lessons learnt that will allow improved data collection for

the future. So even with new generation lidars, for which several improvements were implemented, —partly as a result of the experiences from NORSEWInD reported to the manufacturers—a device may need some care. The final wind observations are the 10-min mean values stored in the MySQL database. The aim of the NORSEWInD project was to observe offshore hub height winds for wind energy and to investigate the wind shear in the marine atmospheric boundary layer. It is easy to imagine many other research applications for which the observations could be useful. The data are available for research upon acceptance by the data owners (contact andy@oldbaumservices.uk for further information).

As discussed in [8] the wind profile LiDAR observations are stand-alone. No other types of observations are available from the platforms. Often information on air temperature, air temperature differences, humidity, boundary-layer height and other parameters are used for in-depth analysis of atmospheric boundary-layer behavior and structures. This is unfortunately not possible with this dataset except if combined with other data sources such as numerical model results, satellite data or other sources as in [38,39].

Conclusions

The long-term performance consistency of wind profiling lidars used for offshore wind energy application has proven excellent. The devices operated offshore from around six months to more than two years. The so-called "NORSEWInD standard", where part of the criteria is that the slope of the linear regression should be within 0.98 and 1.01 and the linear correlation coefficient (R^2) should be >0.98 for the wind speed range 4–16 ms^{-1}, was used for the pre-deployment validation at Høvsøre comparing wind profiling lidar data to observation from a tall meteorological mast at 60, 80, 100 and 116 m. Five lidars passed the standard, two failed slightly whereas one device failed on several criteria. The post-deployment validation of four LiDAR showed excellent performance. The maintenance offshore was sparse but despite this and the harsh environment, the system availability was on average 95% out of a total of 127 months. The data availability was on average 89%. The system and data availability will have to be improved to obtain bankable offshore wind resource data. This is work for the future and most likely will be reached with a combination of improved devices and improved installation, operation and maintenance offshore.

The flow distortion on the offshore platforms was estimated to be insignificant for the LiDAR wind profile observations at hub height. Both CFD modeling and wind tunnel experiments with sub-scale models indicated this. The deployment of wind profiling lidars on large offshore structures appears suitable when the aim is to observe hub height winds at around 100 m AMSL. In contrast, the lidar wind data observed on the coast needed correction for the influence of the terrain as estimated by the flow model in WAsP Engineering and comparing the results to the lidar observations.

We were able to estimate the vertical wind shear distributions, based on the shear exponent of the power law, at several NORSEWInD wind LiDAR nodes and found a very broad range of values, peaking very close to zero, which contrasts with the commonly used constant value offshore of 0.2. This broad range of values is partly due to variation of the vertical wind shear with height, surface

roughness (and thus sea state), and atmospheric stability, and partly to the atmosphere dynamics, which is not accounted for in many wind prediction models.

The shear profiles determined allowed the Weibull A and k and the power density contours in the Baltic Sea east of Denmark to be determined from satellite remote sensing data. The data produced compared well with data measured at co-located meteorological masts.

Acknowledgements

EU-NORSEWInD project funding TREN-FP7EN-219048 is acknowledged. Collaboration with DONG energy, Statoil Hydro ASA, TAQA, Shell UK, Talisman Energy, Kinsale Energy, Scottish Enterprise, Scottish and Southern Renewables, SSE and 3E is kindly acknowledged.

References

1. Wagner, R.; Antoniou, I.; Pedersen, S.M.; Courtney, M.S.; Jørgensen, H.E. The influence of the wind speed profile on wind turbine performance measurements. Wind Energy **2009**, 12, 348–362.
2. Peña, A.; Hasager, C.B.; Gryning, S.; Courtney, M.; Antoniou, I.; Mikkelsen, T. Offshore wind profiling using Light Detection and Ranging Measurements. Wind Energy **2009**, 12, 105–124.
3. Hahmann, A.N.; Lange, J.; Peña, A.; Hasager, C.B. The NORSEWInD Numerical Wind Atlas for the South Baltic; DTU Wind Energy E-0011 (EN); DTU Wind Energy, Roskilde, Denmark, 2012; p. 53.
4. Smith, D.A.; Harris, M.; Coffey, A.S.; Mikkelsen, T.; Jorgensen, H.E.; Mann, J.; Danielian, G. Wind lidar evaluation at the danish wind test site in hovsore. Wind Energy **2006**, 9, 87–93.
5. Kindler, D.; Oldroyd, A.; Macaskill, A.; Finch, D. An eight month test campaign of the Qinetiq ZephIR system: Preliminary results. Meteorol. Z. **2007**, 16, 479–489.
6. Antoniou, I.; Jørgensen, H.E.; Mikkelsen, T.; Frandsen, S.; Barthelmie, R.; Perstrup, C.; Hurtig, M. Offshore Wind Profile Measurements from Remote Sensing Instruments. In Proceedings of the European Wind Energy Association Conference & Exhibition in Athens, Athens, Greece, 27 Feb-3 March 2006.
7. NORSEWInD. Available online: http://www.norsewind.eu (accessed on 3 September 2014).
8. Peña, A.; Mikkelsen, T.; Gryning, S.-E.; Hasager, C.B.; Hahmann, A.; Badger, M.; Karagali, I.; Courtney, M. Offshore Vertical Wind Shear: Final Report on NORSEWInD's Work Task 3.1; DTU Wind Energy-E-Report-0005(EN); DTU Wind Energy, Roskilde, Denmark, 2012; p. 116.
9. Stickland, M.; Scanlon, T.; Fabre, S.; Oldroyd, A.; Mikkelsen, T. Measurement and simulation of the flow field around a triangular lattice meteorological mast. Journal of Energy and Power Engineering. 13, **2013**.
10. Badger, M.; Badger, J.; Nielsen, M.; Hasager, C.B.; Peña, A. Wind class sampling of satellite SAR imagery for offshore wind resource mapping. J. Appl. Meteorol. Climatol. **2010**, 49, 2474–2491.
11. Berge, E.; Hasager, C.B.; Bredesen, R.E.; Hahmann, A.; Byrkjedal, O.; Peña, A.; Kravik, R.; Harstveit, K.; Costa, P.; Oldroyd, A. NORSEWIND—Mesoscale Model Derived Wind Atlases for the Irish Sea, the North Sea and the Baltic Sea. In European Wind Energy Association Confernce, Vienna, Austria, 4–7 February 2013; pp. 1–6.

12. Hasager, C.B.; Badger, M.; Peña, A.; Larsen, X.G.; Bingol, F. SAR-Based wind resource statistics in the Baltic sea. Remote Sens. **2011**, 3, 117–144.
13. Karagali, I.; Hoyer, J.; Hasager, C. SST diurnal variability in the North Sea and the Baltic sea. Remote Sens. Environ. **2012**, 121, 159–170.
14. Karagali, I.; Peña, A.; Badger, M.; Hasager, C. Wind characteristics in the North and Baltic Seas from the QuikSCAT satellite. Wind Energy **2012**, doi: 10.1002/we.1565.
15. Karagali, I.; Badger, M.; Hahmann, A.; Peña, A.; Hasager, C.; Sempreviva, A.M. Spatial and temporal variability in winds in the Northern European Seas. Renew. Energy **2013**, 57, 200–210.
16. ZephIR©. Available online: http://www.zephirlidar.com (accessed on 3 September 2013).
17. Pitter, M.; Slinger, C.; Harris, M. Introduction of Continous-Wave Doppler Lidar. In Remote Sensing for Wind Energy; Peña, A., Hasager, C.B., Lange, J., Anger, J., Badger, M., Bingöl, F., Bischoff, O., Cariou, J.-P., Dunne, F., Emeis, S., et al., Eds.; DTU Wind Energy-E-Report-0029(EN); DTU Wind Energy, Roskilde, Denmark, 2013; pp. 72-103. WindCube©. Available online: http://www.leosphere.com (accessed on 3 September 2013).
18. Cariou, J.-P. Pulsed Lidars. In Remote Sensing for Wind Energy; Peña, A., Hasager, C.B., Lange, J., Anger, J., Badger, M., Bingöl, F., Bischoff, O., Cariou, J.-P., Dunne, F., Emeis, S., et al., Eds.; DTU Wind Energy-E-Report-0029(EN); DTU Wind Energy, Roskilde, Denmark, 2013; pp. 104–121.
19. Sonnenschein, C.M.; Horrigan, F.A. Signal-to-Noise relationships for Coaxial Systems that heterodyne backscatter from atmosphere. Appl. Opt. **1971**, 10, 1600–1604.
20. Menter F.R.; Kuntz M.; Langtry, R. Ten Years of Industrial Experience with the SST Turbulence Model. In Turbulence, Heat and Mass Transfer 4; Hanjalic, K., Nagano, Y., Tummers, M., Eds.; Begell House Inc.: New York, NY, USA, 2003; pp. 625–632.
21. Courtney, M.; Wagner, R.; Lindelöw, P. Testing and Comparison of Lidars for Profile and Turbulence Measurements in Wind Energy. In IOP Conference Series Earth and Environmental Science; Risø National Laboratory, DTU, Denmark, 2008; pp. U172–U185.
22. Stickland, M.; Scanlon, T.; Fabre, S. Computational and Experimental Study on the Effect of Flow Field Distortion on the Accuracy of the Measurements made by Anemometers on the Fino3 Meteorological Mast. In Proceedings of EWEA Offshore: Moving Ahead of the Energy Curve, Amsterdam, The Netherlands, 29 Nov – 1 Dec 2011.
23. Bingöl, F.; Mann, J.; Foussekis, D. Conically scanning lidar error in complex terrain. Meteorol. Z. (Ger.) **2009**, 18, 189–195.
24. Bingöl, F.; Mann, J.; Foussekis, D. Lidar Error Estimation with WAsP Engineering. In Proceedings of 14th International Symposium for the Advancement of Boundary Layer Remote Sensing IOP Publishing IOP Conf. Series: Earth and Environmental Science, Risø National Laboratory, DTU, Denmark, 23-25 June 2008, 2009; Volume 1.
25. Bradley, S.; Mikkelsen, T. LIDAR remote sensing. Int. Sustain. Energy Rev. **2011**, 5, 2–7.
26. Bradley, S.; Perrott, Y.; Behrens, P.; Oldroyd, A. Corrections for wind-speed errors from sodar and lidar in complex terrain. Bound. Layer Meteorol. **2012**, 143, 37–48.

27. Mann, J.; Ott, S.; Jørgensen, B.H.; Frank, H.P. WAsP Engineering 2000; Technical Report Risø-R-1356(EN); Risø National Laboratory for Sustainable Energy, Technical University of Denmark: Risø DTU, Roskilde, Denmark, 2002; Volume R–1356(EN), p. 101.
28. Mortensen, N.G.; Heathfield, D.N.; Myllerup, L.; Landberg, L.; Rathmann, O. Getting Started with WAsP 9; Report Risø-I-2571(EN) ; Risø National Laboratory for Sustainable Energy, Technical University of Denmark: Risø DTU, Roskilde, Denmark, 2007; p. 72.
29. Peña, A.; Hahmann, A.; Hasager, C.B.; Bingöl, F.; Karagali, I.; Badger, J.; Badger, M.; Clausen, N. South Baltic Wind Atlas; Report Risø-R-1775(EN); Risø National Laboratory for Sustainable Energy, Technical University of Denmark: DTU Wind Energy, Roskilde, Denmark, 2011; p. 66.
30. Draxl, C.; Hahmann, A.N.; Peña, A.; Giebel, G. Evaluating winds and vertical wind shear from weather research and forecasting model forecasts using seven planetary boundary layer schemes. Wind Energy 2012, doi: 10.1002/we.1555
31. Emeis, S. Wind Energy Meteorology—Atmospheric Physics for Wind Power Generation. In Series: Green Energy and Technology; Springer: Heidelberg, Germany, 2012; p. 14–196.
32. Cañadillas, B.; Neumann, T.; Raasch, S. Getting a Better Understanding of the Offshore Marine Boundary Layer: Comparison between Large Eddy Simulation and Offshore Measurement Data with Focus on Wind Energy Application. In Proceedings of the Fifth International Symposium on Computational Wind Engineering (CWE2010), Chapel Hill, NC, USA, 23-27 May 2010.
33. Zoumakis, N.M. The dependence of the power-law exponent on surface roughness and stability in a neutrally and stably stratified surface boundary layer. Atmósfera **1993**, 6, 79–83.
34. Westerhellweg, A.; Cañadillas, B.; Beeken, A.; Neumann, T. One Year of Lidar Measurements at FINO1-Platform: Comparison and Verification to Met-Mast Data. In Proceedings of 10th German Wind Energy Conference DEWEK 2010, Bremen, Germany, 17–18 November 2010.
35. Muñoz-Esparza, D.; Canadillas, B.; Neumann, T.; van Beeck, J. Turbulent fluxes, stability and shear in the offshore environment: Mesoscale modelling and field observations at FINO1. J. Renew. Sustain. Energy **2012**, 4, 063136:1–063136:16.
36. Lang, S.; McKeogh, E. LIDAR and SODAR measurements of wind speed and direction in upland terrain for wind energy purposes. Remote Sens. **2011**, 3, 1871–1901.
37. Takeyama, Y.; Ohsawa, T.; Yamashita, T.; Kozai, K.; Muto, Y.; Baba, Y.; Kawaguchi, K. Estimation of offshore wind resources in coastal waters off Shirahama using ENVISAT ASAR images. Remote Sens. **2013**, 5, 283–2897.
38. Takeyama, Y.; Ohsawa, T.; Kozai, K.; Hasager, C.B.; Badger, M. Effectiveness of WRF wind direction for retrieving coastal sea surface wind from synthetic aperture radar. Wind Energy **2012**, doi: 10.1002/we.1526.
39. Bay Hasager, C.; Stein D.; Courtney M.; Peña A.; Mikkelsen T,; Stickland M.; Oldroyd A. Hub Height Ocean Winds over the North Sea Observed by the NORSEWInD Lidar Array: Measuring Techniques, Quality Control and Data Management. Remote Sensing 2013, vol (5)
40. Bay Hasager C et al. SAR – Based wind resource statistics in the Baltic Sea. Remote sensing 2011, 3. 117-144